UCRL-ID-147604

An Inner-Shell Photo-Ionized X-Ray Laser at 45 Å

F. A. Weber, P. M. Celliers, S. J. Moon, R. A. Snavely, L. B. Da Silva

February 1, 2002

U.S. Department of Energy

Lawrence Livermore National Laboratory

Approved for public release; further dissemination unlimited

DISCLAIMER

This document was prepared as an account of work sponsored by an agency of the United States Government. Neither the United States Government nor the University of California nor any of their employees, makes any warranty, express or implied, or assumes any legal liability or responsibility for the accuracy, completeness, or usefulness of any information, apparatus, product, or process disclosed, or represents that its use would not infringe privately owned rights. Reference herein to any specific commercial product, process, or service by trade name, trademark, manufacturer, or otherwise, does not necessarily constitute or imply its endorsement, recommendation, or favoring by the United States Government or the University of California. The views and opinions of authors expressed herein do not necessarily state or reflect those of the United States Government or the University of California, and shall not be used for advertising or product endorsement purposes.

This work was performed under the auspices of the U. S. Department of Energy by the University of California, Lawrence Livermore National Laboratory under Contract No. W-7405-Eng-48.

This report has been reproduced directly from the best available copy.

Available electronically at http://www.doc.gov/bridge

Available for a processing fee to U.S. Department of Energy
And its contractors in paper from
U.S. Department of Energy
Office of Scientific and Technical Information
P.O. Box 62
Oak Ridge, TN 37831-0062
Telephone: (865) 576-8401
Facsimile: (865) 576-5728
E-mail: reports@adonis.osti.gov

Available for the sale to the public from
U.S. Department of Commerce
National Technical Information Service
5285 Port Royal Road
Springfield, VA 22161
Telephone: (800) 553-6847
Facsimile: (703) 605-6900
E-mail: orders@ntis.fedworld.gov
Online ordering: http://www.ntis.gov/ordering.htm

OR

Lawrence Livermore National Laboratory
Technical Information Department's Digital Library
http://www.llnl.gov/tid/Library.html

A Final Report to the Laboratory Directed Research and Development Committee on Project 99-LW-042: "An Inner-Shell Photo-Ionized X-Ray Laser at 45 Å"

Principle Investigator
Franz A. Weber

Co-Investigators
Peter M. Celliers, Stephen J. Moon, Richard A. Snavely, and Luiz B. Da Silva[a]

Lawrence Livermore National Laboratory
Livermore, CA 94550, USA

[a] Pearl Technology Holdings
1409 N. Ft. Harrison, Unit A
Clearwater, FL 33755, USA

Abstract

This report summarizes the major accomplishments of this three-year Laboratory Directed Research and Development (LDRD) Lab Wide (LW) project entitled, "An Inner-Shell Photo-Ionized X-Ray Laser at 45 Å", tracking code 99-LW-042. The most significant accomplishments of this project include the design of a suitable x-ray laser target, the invention of a measurement technique for the determination of rise times of x-ray pulses on the order of 50 femtoseconds, and a novel setup for generating a traveling wave with an ultrashort optical laser pulse. The pump probe technique for rise time measurement will allow us to detect ultrashort x-ray pulses, whose generation by means of a variety of 4^{th} generation light sources is currently under planning elsewhere.

1. Introduction

Long before lasers capable of generating x-rays were developed, researchers had already proposed a whole host of applications and anticipated their benefits in biology, biomedical imaging, specifically microscopy and holography, materials science, and plasma physics. For laboratory x-ray laser scientists it has been a long standing goal to demonstrate an x-ray laser working at wavelengths close to or even below the water window (26 Å – 44 Å) using a table-top energy source.

Since the first demonstration of x-ray lasing at Lawrence Livermore National Laboratory in 1985 [1], and elsewhere [2], based on the utilization of high-power pump lasers designed and built for fusion research, new and more efficient pumping techniques have been vigorously sought after. In the last decade, many important experiments have been conducted and good progress has been made towards table-top x-ray lasers, which would warrant giving serious thought to applications mentioned above. The advent of a new generation of chirped pulse amplification techniques has made possible the design and fabrication of powerful and ultra-short pulse duration pump lasers that seem to have the capability to shrink source dimensions from occupying whole rooms to table-top size. Most of these applications, however, do indeed require x-ray laser wavelengths shorter than currently attainable with table-top sized schemes since scaling to wavelengths shorter than 100 Å proves rather difficult [3] – [7].

Beginning from Fiscal Year (FY) 1999, we have carried out a Laboratory Directed Research and Development (LDRD) project, entitled "An Inner-Shell Photo-Ionized X-Ray Laser at 45 Å". The aim of this project, funded by the Laboratory Wide branch of the program, was to study the design and, eventually, the properties of an x-ray laser, based on a scheme that to date has not been demonstrated. We benefited from advances in the field of soft x-ray optics [8] as it allowed us to design a versatile spectrometer for measuring x-ray converter backside emission.

This LDRD project was completed in FY2001, delivering a thoroughly modeled x-ray laser target with backside emission statically characterized on prototype assemblies. In addition, we have invented a novel technique to measure the slew rate of ultrafast x-ray pulses as well as a method to produce an ultrashort laser pulse at line focus in a traveling wave configuration. The former uses a diamond as an x-ray transducer and an interferometer to determine rise times of these x-ray flashes while the latter employs a holographically created grating and a combination of spherical and cylindrical optics to relay image the grating surface onto the target. Both these techniques will allow us to shoot x-ray laser targets at an appropriate short pulse facility capable of delivering the required amount of energy per pulse with maximum contrast.

The impact of this project is recognized in the international physics communities, particularly those pursuing new x-ray and gamma ray laser schemes, resulting in a number of invited lectures at international physics conferences. This report represents a concise summary of the technical achievements of this LDRD-funded project. For more detailed information on conference presentations and records of invention the readers are directed to the Appendix of this publication. Here, in section 2 we discuss physics of the target and present our modeling results. We describe our method for a traveling wave setup suitable to pump inner-shell photo-ionization schemes in section 3. The description of the scheme for rise time measurements of ultrafast x-ray pulses can be found in section 4. The report on our experimental findings on target output and laser performance is given in section 5. We summarize and detail our future plans in section 6.

2. Target Physics

For this project we have decided to pursue a class of x-ray lasers previously unrealized and first proposed by Duguay and Rentzepis [9]. Several authors have since adopted that inner-shell photo-ionization scheme [10], [11], and conclude that operating on a Kα transition of a low Z element constitutes an attractive way to efficiently pump an x-ray laser in the sub 50 Å regime. All these new schemes still need sub 50 femtosecond and greater than 1 J in an optical pulse to drive the transition. Advances in powerful

ultrashort pulse laser (USPL) technology prompted us to investigate that group of schemes with the application of carbon as the lasant material in greater detail. The choice of this material is by virtue of its electronic properties with particular respect to the Auger recombination rate. We begin by examining the dynamic physical processes in carbon, which will yield Kα radiation at a wavelength of 45 Å.

Pumping a 2p – 1s transition in carbon requires an ultrashort pulse, broad-bandwidth (incoherent) x-ray source with additional filtering in order to preferentially ionize the inner shell (1s) electrons. The basic concept relies on the fact that the photo-ionization cross-section is much larger for the tightly bound inner shell electrons (i.e., the 1s electrons) than for the more loosely bound outer shell electrons (i.e., the 2p and 2s electrons) as depicted in figure 1. This requires photon energies at least high enough to photo-ionize the K-shell, more than approximately 283 eV, in the case of carbon. As a consequence of the higher cross section, the inner-shell electrons (1s electrons) are "selectively" knocked out, leaving a hole state $1s2s^22p^2$ in the singly charged ion (C^+) and resulting in a population inversion relative to the radiatively connected state $1s^22s^22p$ in C^+, leading to gain on the 1s-2p transition at 45 Å. As only the single ionization state is involved, and the lasing transition is of resonant character, this scheme intrinsically provides much higher quantum efficiency than other schemes.

There are several competing processes that deplete the population inversion, including auto-ionization, Auger decay, and in particular collisional ionization through ejection of the outer-shell electrons by electrons generated during photo-ionization. These competing processes rapidly quench the gain. Consequently, the pump method must be capable of populating the inversion at a rate faster than the competing processes. This requirement can be met by utilization of an ultra-fast, high intensity laser impinging on highly absorptive material. Under the proper conditions, that process can generate an ultra-fast, bright x-ray source [12], [13]. For the carbon 2p-1s lasing transition investigated here, an ultra-fast x-ray burst (on the order of 80 fs) is needed to generate theoretically predicted gain of approximately 16 cm^{-1} with duration of 50 fs [14]. Although the concept of the ISPI laser was proposed 30 years ago, it has never been demonstrated because such

pumping sources have not been available. Only more recent advances in laser technology using the chirped-pulse amplification technique have brought in sight multi terawatt and even petawatt lasers [15]. Based on this significant progress, an x-ray laser produced through the implementation of the inner-shell photo-ionization scheme as detailed above for the carbon K shell at 45 Å has a significant probability of success. The level diagram showing the lasing transition is given in figure 2.

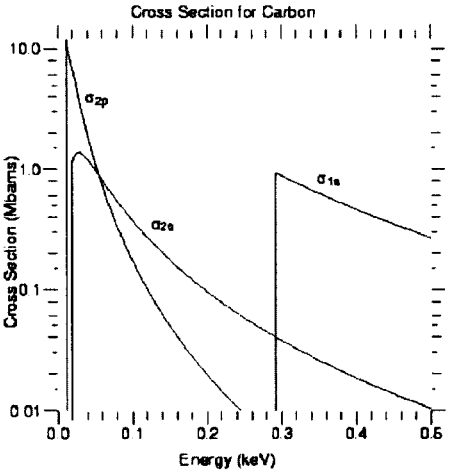

Figure 1: Photo-ionization cross-section for carbon.

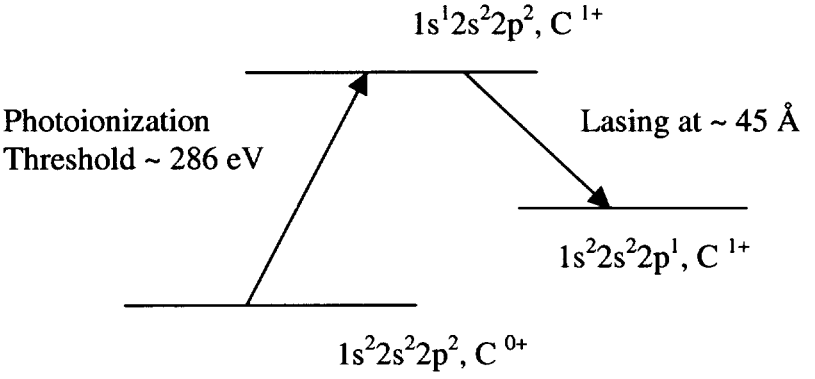

Figure 2: Level diagram of the carbon inner-shell photo-ionization laser.

2.1 Target Design

Our initial work focused on the basic target design. In previous photo pumping experiments, the pumping source was generally located within the lasing medium. In our case, a filtered x-ray source is necessary, requiring a new design. As depicted in figure 3, the target comprises a multilayer structure with the x-ray source converting the optical (laser) energy into x-rays on one side, and the lasing material, i.e., low density carbon, on the other side, separated by a filter of low-Z material (e.g., Be) with an appropriate thickness. For laser driven x-ray sources, experimental studies have shown that microstructured high-Z targets could potentially serve for this purpose [16] – [19]. This group of designs may include cluster targets (e.g., gold black), grooved targets, and microcylinder targets. An alternative target design employs a thin Zn layer that can function both, as the x-ray source and the filter. This design simplifies the target fabrication and may avoid the absorption due to the unheated high-Z material in the above design.

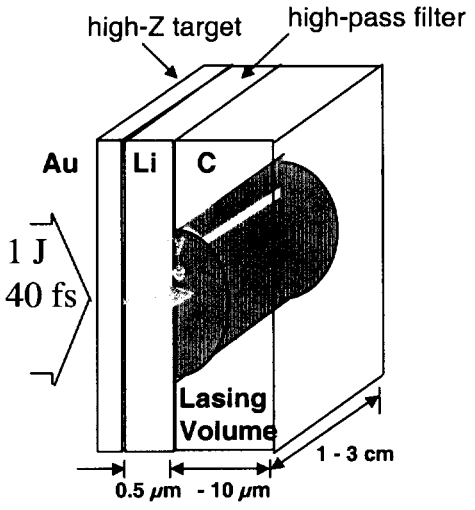

Figure 3: Schematic of initial target investigated.

Our first approach, illustrated in figure 3, followed a traditional design of the pumping mechanism, which uses a Au target as the high Z source. Filtering of the resulting broad x-ray spectrum is done through a low Z element such as Be or Li. During the course of this investigation, however, we have found that via the effect of self-filtering from the cold part of the target material we can eliminate the low energy x-rays. While examining a variety of alternate target designs, we concluded that utilization of a single thin foil of the medium Z element Ti, instead of a low Z filter such as Be, also allows for high gain in the lasant. The resulting incoherent x-ray source is insensitive to heating of the filter material. In addition, this improved target design offers the advantages of less toxicity and significant simplifications in the target fabrication process.

2.2 Simulations

Results of our modeling effort are shown in figures 4 a through c. An USP high intensity optical laser of $1x10^{17}$ W/cm^2 and 40 fs pulse duration is incident on a foil consisting of 200 Å layered on 1000 Å of Ti. The laser is at normal incidence on the gold absorber, the front side of the target, and the incoherent x-ray source, which pumps the carbon lasant, is due to back-side emission. The modeling was performed using the hydrodynamics/atomic code LASNEX [20]. The code includes many physics models necessary to simulate a multidimensional radiative hydrodynamics problem, including laser-matter interaction, radiation transfer, electron thermal diffusion by conduction, and simple description of non-local thermodynamic equilibrium atomic kinetics. Reference 20 includes a description of the physics models used in LASNEX.

The energy from the optical laser is deposited in a self-consistent manner by solving the wave equation for the laser electro-magnetic field and the atomic kinetics and x-ray emission are calculated with an average-atom atomic model, which includes spin orbit coupling. Careful optimization of the converter/filter assembly parameters yielded the values indicated above. Furthermore, the ionization velocity in the absorber material ensures that the thin gold layer is completely ionized at the end of a ~ 40 fs optical pump pulse, and at the same time the absorption occurs at near solid density. Figure 4 a shows the calculated backside emission from the foil structure and figure 4 b shows the

corresponding gain of 9.9 cm^{-1} for low-density carbon foam at 10^{18} cm^{-3}. Figure 4 c depicts spectral emission from the target structure for various times.

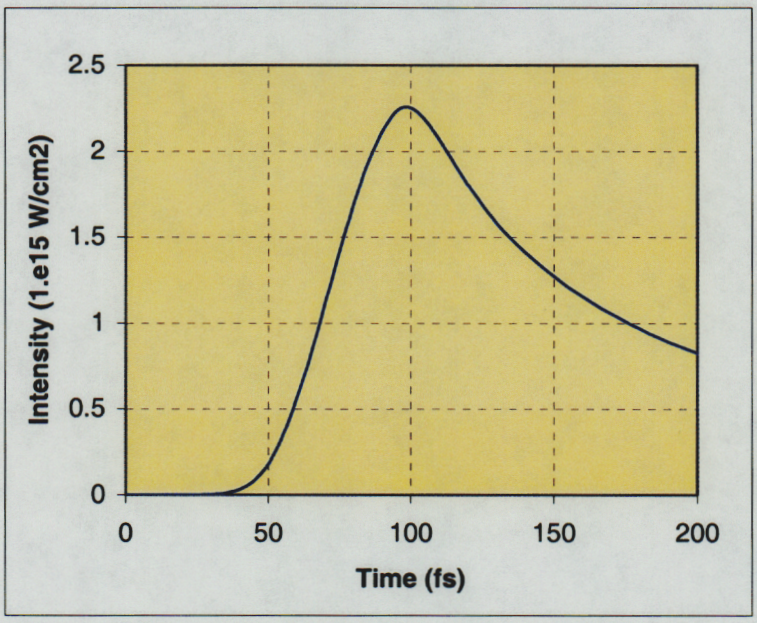

Figure 4 a: Simulated temporal history of the source, spectrally integrated.

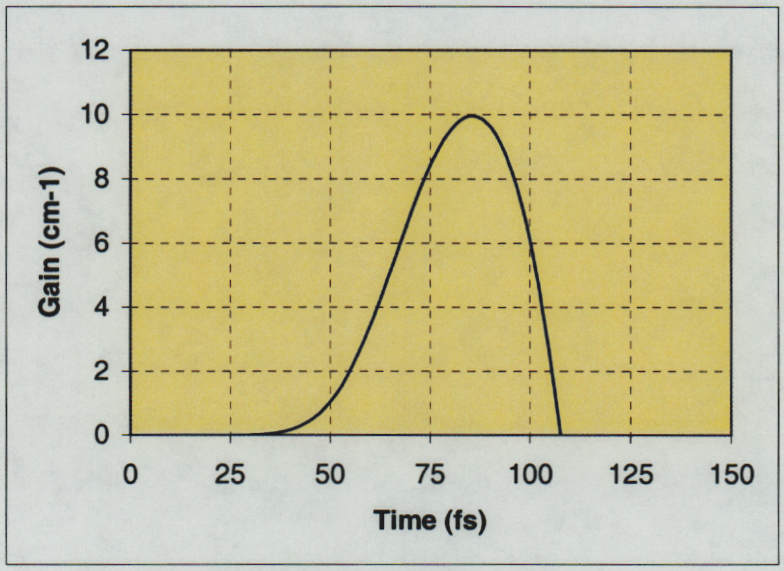

Figure 4 b: Calculated gain in carbon lasant (10^{18} cm^{-3} foam) at 45 Å.

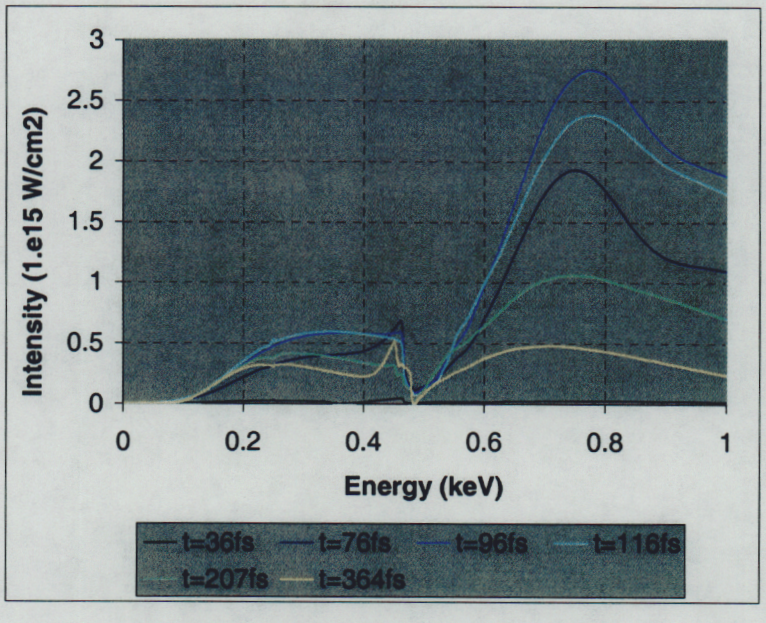

Figure 4 c: Calculated spectral emission for various times.

As evident from figures 4 a through c, the majority of x-ray energy is emitted above the carbon K-edge, whereas the long wavelength x-rays are sufficiently suppressed by the titanium layer. The integrated flux shows a rise time on the order of 50 fs and peaks at around 100 fs. As a consequence the expected gain is also of corresponding short duration.

3. Traveling Wave Pumping of an Ultrashort Pulse X-Ray Laser

The use of traveling optical waves as a method of delivering optical energy is not new to laser science [21] – [25]. Even before chirped pulse amplification (CPA) came on the scene, Bor [6] employed a traveling wave technique to produce optical pulses with a 1 picosecond duration. Indeed, the field of collisionally pumped XRLs has also seen the implementation of traveling wave pumping (TWP) schemes, although at much longer pulse durations, in order to enhance XRL performance. Previous analysis [27] for these schemes shows that TWP may be advantageously applied whenever the pump time divided by the target length turns out to be less than 33 ps/cm.

The physical characteristics of the required traveling wave optical pumping system are largely determined by the physics of the x-ray laser transition as described in section 2. The very rapid rise time of the broad-bandwidth x-ray source, faster than the upper state lifetime in carbon, dictates, because of the competing processes and subsequent depopulation of the lower laser state, zero gain for times greater than approximately 80 fs (see figure 4 b). This time constraint is true for every incremental length of the lasing volume. Thus, we find that the stringent pump requirements of the ISPI XRL scheme as a consequence also impose very stringent requirements on the quality and fidelity of the focusing system. A traveling wave focusing scheme is therefore essential to pump an XRL amplifier target.

The pump light (optical energy of USPL) must be delivered to the target at an intensity of 1.0×10^{17} W/cm^2 in a spot size of approximately 30 μm that illuminates the target along a linear track of ~ 10 mm length and traveling at the velocity of light *c* (index of refraction ~ 1.000) along the target surface. The arrival time deviation from a linear variation at any point along the trajectory must be less than 50 fs corresponding to a distortion level around 10^{-4} or better. The pulse duration of the focused beam must be a faithful representation of the incident pulse from the drive laser. Also attendant is the vertical spatial distortion that, accordingly, must be limited to better than +/- 15 μm over 10 mm or ~ 10^{-3} over the laser length. These are not unreasonable numbers for generic optical systems, however, the utilization of a high power USPL with its 50 to 100 nm bandwidth mandates all-reflective optical surfaces in order to eliminate not only the chromatic distortions that lead to pulse temporal broadening [28], but also distortions due to the intensity induced nonlinear index of refraction variations (B-Integral). As a result, only a vacuum diffraction grating succeeds as a dispersive element out of a variety of traditional methods (prisms, Fabry-Perot interferometers, and gratings [29], [30]) to tilt wave fronts of optical pulses by angular dispersion.

The use of an all-reflective optical system leads to constraints of both, the number and the orientation of the surfaces employed to minimize optical aberrations. Path delay methods, as described in [31], analyze the frequency dependent effects of diffraction gratings by means geometrical optics. It is shown that they can be employed for the theoretical treatment of femtosecond optical pulses propagating through dispersive elements. In

previous TWP setups, a combination of pulse tilt angle and target tilt angle resulted in synchronism across the target plane, based on the quasi-monochromatic nature of the laser. With the use of USPL and a rather large 100 nm bandwidth, however, angular dispersion of the grating causes immediate temporal broadening of the pulse. Consequently, one of essentially two methods to tilt an USPL wavefront without disturbing its propagating 0 GVD has to be applied. If a positively chirped pulse is incident on a grating, the dispersive element will impart a negative chirp to the pulse resulting in a 0 GVD plane at some distance from the grating surface, which then may be relay imaged to the target, rendering the target plane also a GVD plane [32].

As part of this project we have developed a solution for meeting the stringent requirements by incorporating several standard optical design elements and a grating to produce a near-diffraction limited line focus on the target. The schematic of the TWP setup is depicted in figure 5. The novel feature of the design is a holographically-generated grating that serves both, to produce the pulse front tilt needed for the traveling wave, and also to correct residual aberrations in the focusing system. We designed the system to project an image of an incident 50 mm beam onto the 10 mm target surface at 5x demagnification. Most of the focusing power is accomplished using a reflective inverted off-axis Schwarzschild microscope configuration (primary mirror: 1500 mm concave radius, secondary mirror: 309 mm convex radius). These two mirrors are placed in a classic Schwarzschild confocal configuration – and the design is optimized for 5:1 demagnification. The grating is centered on, and perpendicular to, the chief axis of the Schwarzschild system; the grating image is then projected onto the target plane, which is also centered on and perpendicular to the chief axis. In our design we use an off-axis subset of the cylindrically symmetric Schwarzschild configuration, hence the rays traveling through our focusing system arrive obliquely on all the optics. In order to produce a pulse front traveling at velocity c across the target surface using an imaging system operating with magnification M, it can be shown that the grating must be illuminated at an angle $\theta = \sin^{-1}(M)$ from the grating normal (while the diffracted beam leaves the grating approximately at the normal). In our case $M = 0.2$ and $\theta = 11.54°$. The pulse front intersects the grating surface along a vertical line; this line must be focused onto the target at a point, which requires the focusing system to be astigmatic.

We accomplish this by using two additional cylindrical mirrors that are configured to produce the required line focus on the target. Using the combination of the two spherical and two cylindrical elements a ray trace analysis can optimize this system to produce a line focus that is a few times diffraction-limited at the target plane. The trajectory of the pulse front produced by imaging a flat grating onto a flat target will not have a constant velocity, but will have a small quadratic deviation from this. (A planar pulse front originating from the grating reaches the target plane as a cylindrical pulse front because it must pass through a focus before reaching the target.) We can adjust the shape of the pulse front to correct for this by using a slightly cylindrical surface at the grating plane. The required grating surface curvature depends on the magnification and focal length of the Schwarzschild system.

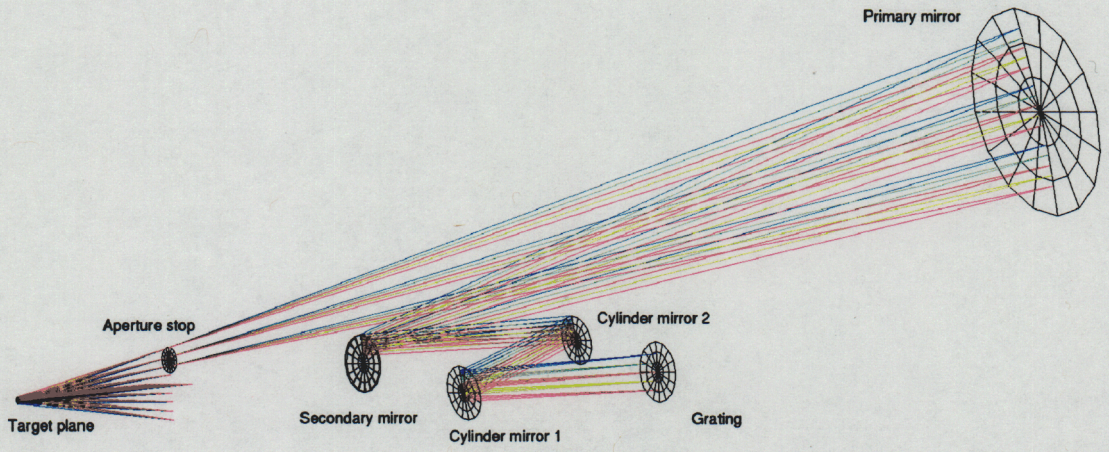

Figure 5: USPL traveling wave pumping system in line focus geometry.

The remaining geometrical aberrations in the system can be corrected by generating the grating holographically. To accomplish this the system must be back-illuminate with a diffraction limited line focus at the target plane. The grating can then be produced by interfering the back propagating beam with the 11.54° incident beam at the grating surface. The back propagating beam incorporates the residual aberrations in the focusing system, thus allowing the production of a grating pattern that will correct for these

aberrations. During operation slight adjustments in the phase velocity of the pump at the target can be accomplished by slight tilts of the grating about an axis perpendicular to the plane of incidence.

4. Measuring the Rise Time of Ultrafast X-Ray Pulses

Conventional high speed x-ray diagnostics (x-ray streak cameras, PIN diodes, diamond PCD devices) do not provide sufficient time resolution in order to resolve the 40 fs x-ray pulse required to achieve level inversion and gain on the inner-shell photo-ionized system. For optimization and study of ultrafast systems in general it is important to have this capability developed. A pump-probe technique is the obvious solution to measuring events where detector resolution is insufficient to resolve the event. We have devised a technique to resolve an ultrafast rise time x-ray pulse using a diamond plate as an x-ray transducer. A sketch of the method is shown in figure 6.

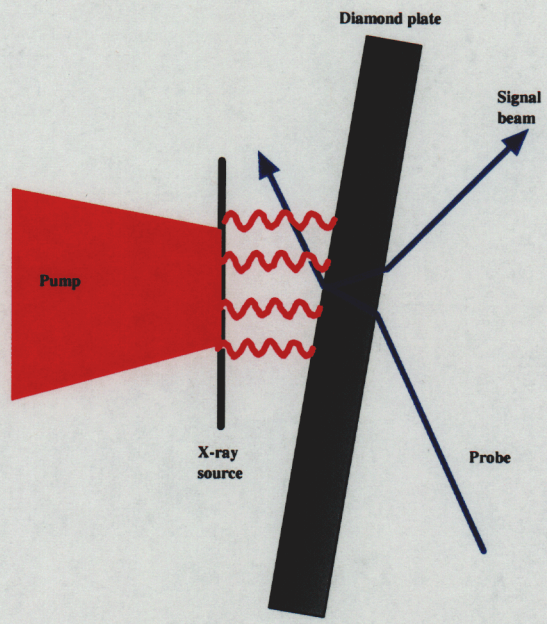

Figure 6: Schematic for time-resolved measurements of x-ray emission.

X-ray energy from the source impinging on the surface of the diamond plate will photo-ionize electrons from inner-shell states and create a transient population of free carriers in the conduction band. These carriers will recombine rapidly through Auger recombination processes. However, calculations show that the transient carrier density will be high enough to modify the optical reflectivity of the interface such that it can be detected by the probe beam. The arrangement employs a p-polarized probe beam entering the diamond plate at Brewster's angle. As is shown in figure 7, with no x-ray interaction the nominal reflectivity at Brewster's angle is zero, and no signal should be registered on the detector. If the probe beam arrives at the sample simultaneously with the pump the surface reflectivity will be modified by the presence of the x-ray-generated free carriers and a stronger reflection can be observed at the interface.

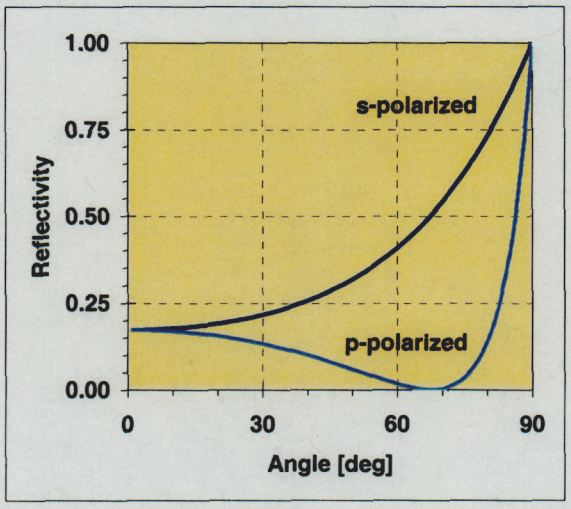

Figure 7: Optical reflectivity function for diamond.

The sample structure can be arranged to encode time-related information spatially by placing the x-ray transducer at a moderate angle relative to the sample. This encodes a linear gradient of arrival times across the sample, which can be extracted by imaging the reflected beam onto a CCD detector array. Utilization of a diamond plate provides increased sensitivity of the measurement around the carbon K absorption edge, which is

the important region of the x-ray emission spectrum with respect to pumping a 2p-1s lasing transition in carbon at 45 Å.

We have theoretically analyzed the physical mechanisms of the pump probe experiment with particular respect to electronic processes in the diamond x-ray transducer by treating the transient electron population as a free electron gas employing the Drude model. The fast x-ray source preferentially releases K-shell electrons into the conduction band. In addition to the photoelectrons there are also Auger electrons, which, through collisions, result in a cascade of electrons into the conduction band. The near surface accumulation of electrons changes the index of refraction, n, and subsequently the reflectivity increases from nominal zero to a detectable level as is shown below. The photo production rate yielding photoelectrons as a result of x-ray source impact is given by,

$$R_{photo} = \int dE\, \sigma_{photo} \Phi(E)$$

where σ_{photo} is the photo-ionization cross-section and $\Phi(E)$ is the incident x-ray flux. The photoelectrons populate the conduction band and additional Auger electrons create further conduction electrons through collisional ionization. Here the rate is given by,

$$R_{electron} = \int dE\, \sigma_{electron} N_e(E) v(E)$$

where $\sigma_{electron}$ is the electo-ionization cross-section and v is the electron velocity and $N_e(E)$ is the number of electrons per unit volume. This ionization creates a transient population in the conduction band. Assuming a Drude model, the dielectric function is given by,

$$\varepsilon(\omega) = 1 - \frac{\omega_p^2}{\omega(\omega - i/\tau)}$$

where

$$\omega_p = \left(4\pi N_e e^2 / m \right)^{1/2}$$

is the plasma frequency, N_e is the free electron density, τ the electronic relaxation time, and m is the reduced mass. The index of refraction,

$$n = \sqrt{\varepsilon}$$

is dependent on the electron density and changes corresponding to the time history in figure 8. The optical reflectivity R=f(Re(n), Im(n)) at the interface is modified and the probe beam at Brewster's angle will yield a non-zero reflected signal on the time scale indicated in figure 9.

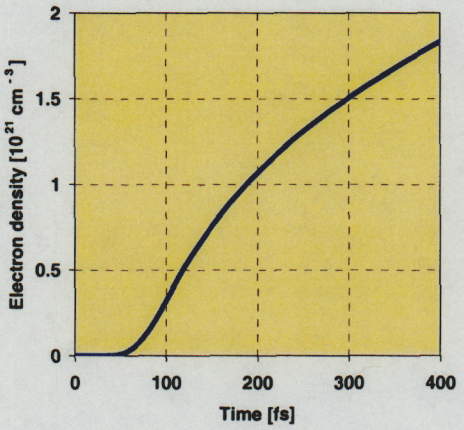

Figure 8: Transient conduction band population in diamond x-ray transducer.

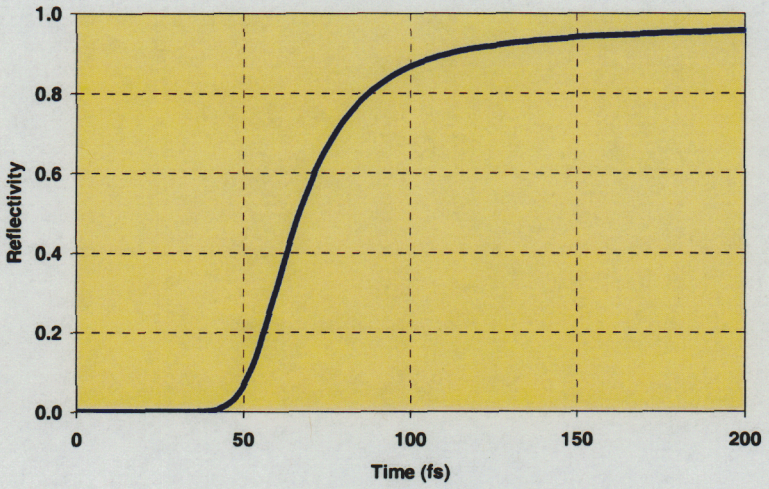

Figure 9: Dynamic response of interface reflectivity.

5. Experimental Results

5.1 Soft X-Ray Spectrometer

In order to effectively and accurately investigate the emission from the x-ray converter it is necessary to field a spectrometer, which covers wavelength regions on both the long and short wavelength side of the carbon K-edge. That requirement puts severe limitations on the choice of materials to be employed in the dispersing element of the detection system. We have designed and built a versatile soft x-ray spectrometer, whose schematic is depicted in figure 10 a.

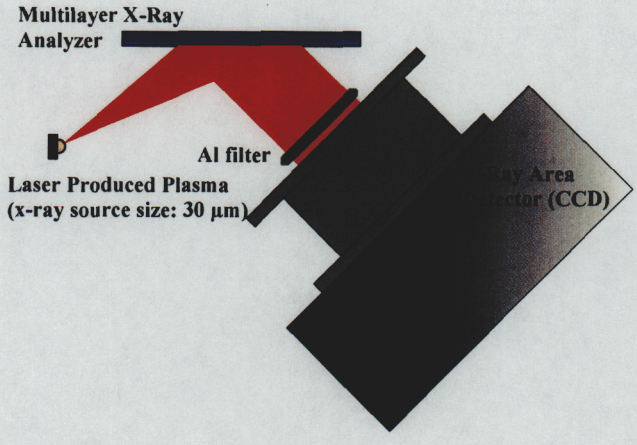

Figure 10 a: Multilayer analyzer based x-ray spectrometer.

The instrument comprises a multilayer-based analyzer as well as a charge coupled device as a position sensitive detector. Backside emission from the target impinges on the analyzer surface at different angles of incidence and according to Bragg's equation different wavelengths are diffracted in one dimension onto an x-ray area detector. We use a dual d-spacing reflector, which allows broad-band coverage of the incident radiation's energy regime. The synthetic crystal comprises a multilayer structure based on a recently developed WC/C and M400/B_4C deposition technique. The artificial layer stack is deposited onto a super-polished slab of silicon oxide with a cross-sectional area of 1" by 3/4 " and 2" in length. The calculated spectral resolution and reflectivity are $5x10^{-2}$ and

15 %, respectively. We have calibrated the system in a self-consistent fashion and found a peak reflectivity of 17 %. The bandpass of the system is shown for in figure 10 b for two layer spacings and a 2" inch length of the dispersing element. Note that a particular source distance automatically dictates both, wavelength range and detector distance. The CCD is a full frame device with three phase clocking configured to an array of 1024 by 1024 pixels with 24 microns by 24 microns individual pixel size. It features a back-thinned and back-illuminated chip with no antireflection coating for improved sensitivity and quantum efficiency in the VUV and soft x-ray regions of the spectrum.

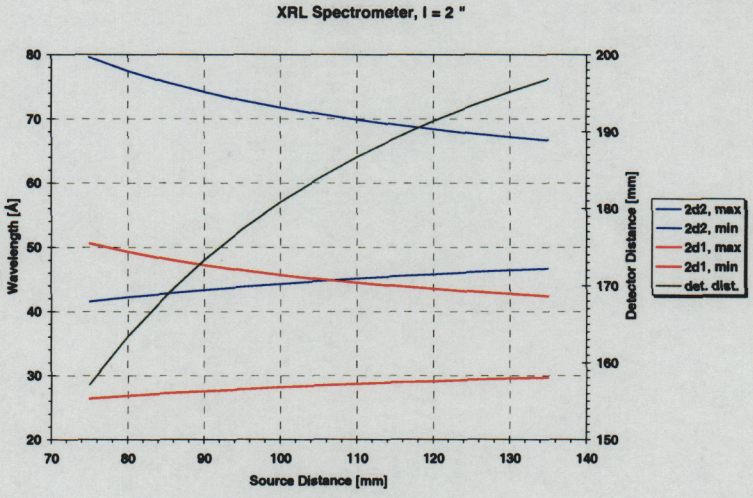

Figure 10 b: Wavelength regions covered by our design.

5.2 Target Backside Emission

The experimental investigation was conducted at the LLNL Falcon USPL facility. The arrangement is depicted in figure 11. The laser is based on a Ti:Sapphire oscillator and uses CPA to produce nominally 500 mJ pulses of 35 fs individual duration at a repetition rate of 1 Hz. We used the laser's regenerative amplifier pumped at saturation level. After initial determination of output levels all shots were set up in a p-polarized configuration and a 45 degree angle of incidence on target was maintained. The center wavelength of the laser λ = 820 nm was focused on target by means of an off-axis

parabola at f/2. In our first set of experiments we have used maximum energy through the four pass amplifier and air compressor and have been able to achieve around 100 mJ on target. On every shot we monitored the unconverted beam energy as well as the level of amplified spontaneous emission (ASE) by means of a calorimeter and a 170 ps fast-rise time photodiode, respectively. A typical ASE profile rose linearly in time until the arrival of the main pulse.

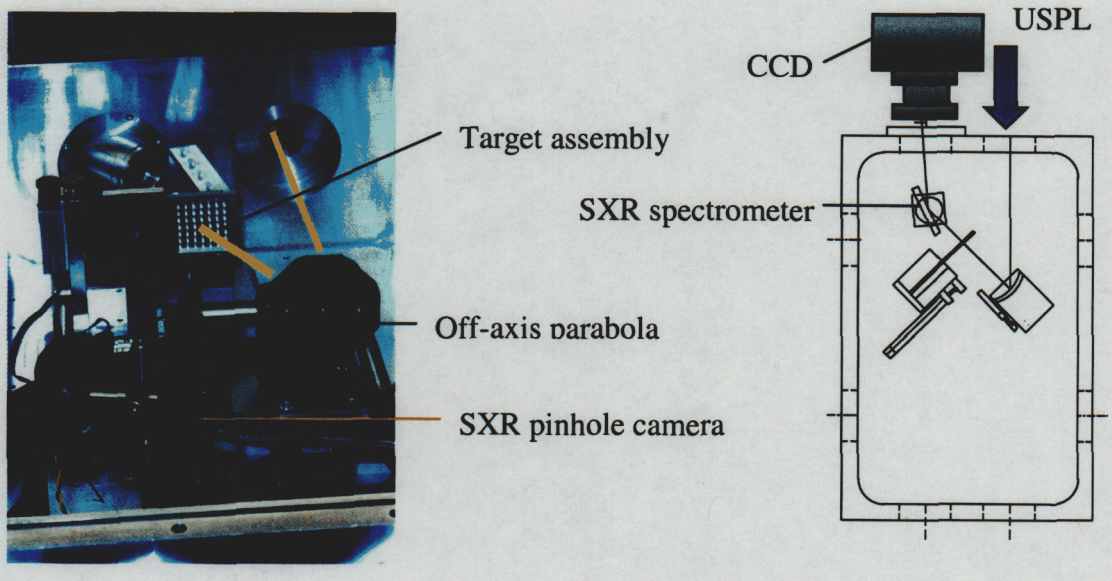

Figure 11: Experimental setup at LLNL's Falcon USPL.

The CCD as well as a soft x-ray pinhole camera (SXR PHC) were filtered in order to block stray light and unwanted optical reflections. We used 12.5 μm of beryllium for the SRX PHC whereas we installed a total of 2kÅ of aluminum on top of 2 kÅ of Lexan in the spectrometer. The spectral composition of backside x-ray emission for various focal distances is shown in figure 12. For verification of the focal spot size on the target front side we employed an x-ray pinhole camera comprising a multiple pinhole array coupled to a soft x-ray sensitive CCD as described above. The diagnostic was operated at a magnification of 15. Data analysis on both, the pinhole images and the static spectroscopy data was performed by subtracting dark images in order to correct for detector temperatur-dependent noise in addition to the subtraction of high energy photon

and electron generated background. We then integrated the signal over the regions of interest and adjusted for analyzer reflectivity, filter transmission functions, and detector quantum efficiency.

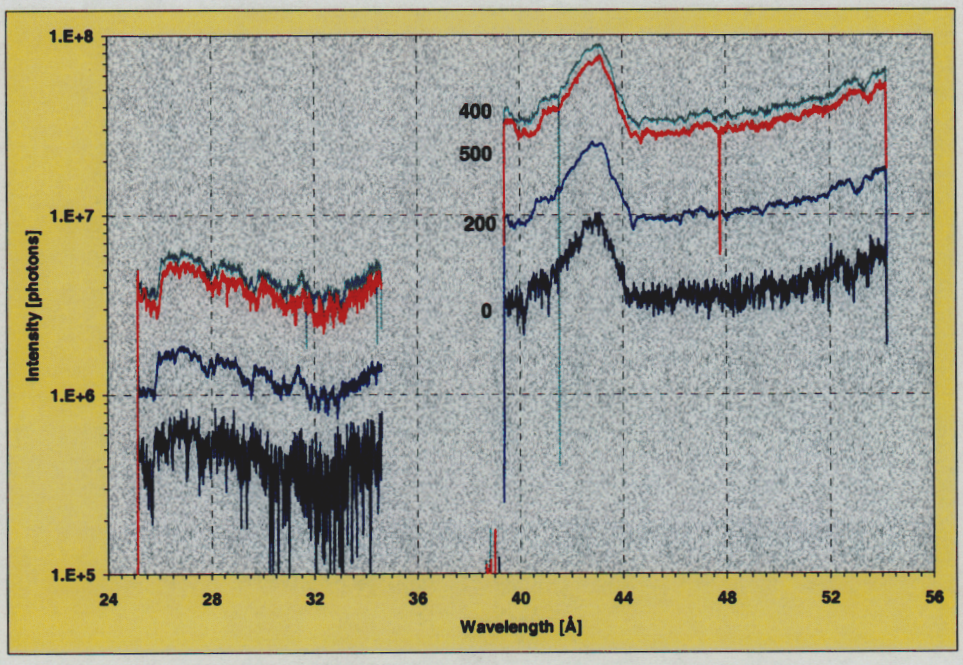

Figure 12: Time integrated backside emission increases away from best focus.

We found the spot size at best focus to be around 23 µm at FWHM, which corresponds to a laser intensity on target of 6.9×10^{17} W/cm^2. The pinhole image is displayed in figure 13. Also note that the best focus is located at a position measuring 100 µm away from the initial target surface due to a distance calibration offset.

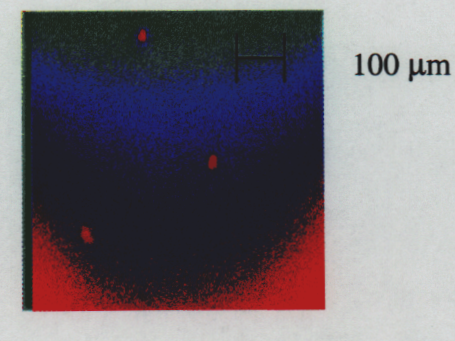

Figure 13: SRX pinhole image at best focus (6.9×10^{17} W/cm^2).

The variation of laser intensity as a function of focal distance for a representative sequence of shots is evident in the series of pinhole images given in figure 14 a. Corresponding intensities are plotted in figure 14 b.

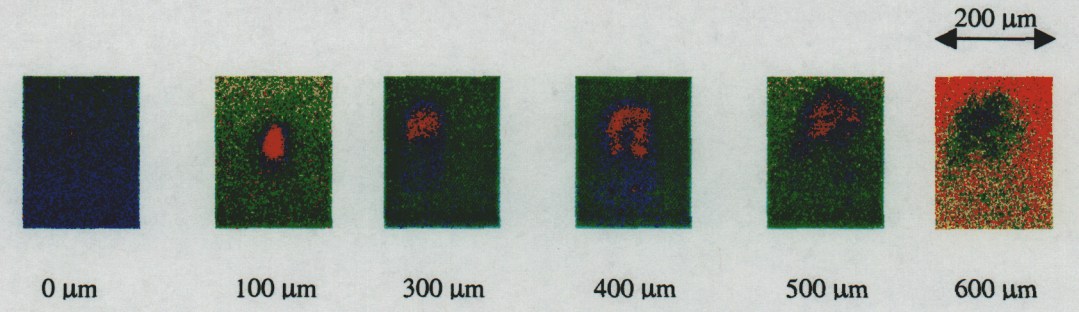

Figure 14 a: Pinhole images for various focal distances.

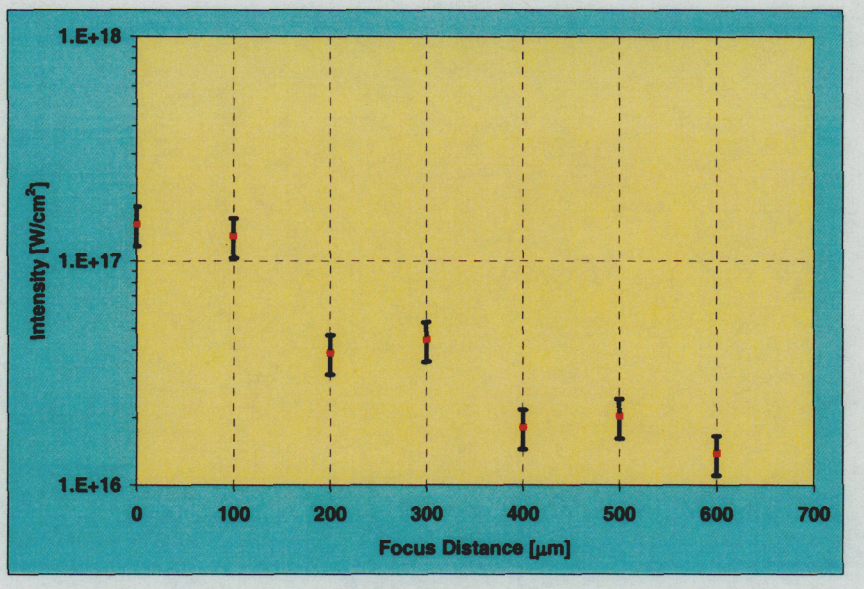

Figure 14 b: Corresponding laser focal spot intensities.

We determined the conversion efficiency η from both, the pinhole images and the integrated spectral emission using the following equations.

$$E_{pulse} \cdot \eta \cdot \Omega_{PH} \cdot T(E) \cdot QE(E) = \sum n_{phot} \cdot E_{phot} = cts \cdot \varepsilon \cdot \xi$$

$$E_{pulse} \cdot \eta \cdot \Omega_{SP} \cdot T(E) \cdot QE(E) = \int_E n_{phot} \cdot dE_{phot} = cts \cdot \varepsilon \cdot \xi$$

E_{pulse} denotes the energy per pulse, Ω the solid angle subtended by the respective diagnostic, T(E) the filter transmission function, QE (E) the detection system quantum efficiency, n_{phot} the number of photons in the energy interval dE_{phot}, cts the digital CCD counts, ε the mean ionization energy in the semiconductor material, and ξ the number of photoelectrons per digital count. We found the best conversion efficiency at maximum backside emission around 300 μm away from best focus at 1.2×10^{-4}. We tend to attribute the worse efficiency at best focus to high plasma temperature.

5.3 Prepulse Experiments

Near-solid-density plasmas not only have parameters relevant to inertial confinement fusion, but are also regarded as being sources of short-pulse x-rays [33], [34]. The physics of high intensity laser interactions with solid targets is therefore of wide interest. At laser intensities above 10^{15} W/cm^2, collisionless processes such as resonance absorption [35] and vacuum heating [36] begin to dominate the laser absorption mechanisms. Both of these mechanisms are highly sensitive to the electron density scale length $L = [(1/n_e)(dn_e/dx)]^{-1}$ at the interaction surface, and therefore a prepulse can strongly affect the primary interaction if a preformed plasma is created. By utilization of a short-duration, intentional prepulse, however, one can experimentally vary the plasma scale length [37]-[39].

We have designed and implemented an interferometer at the Falcon USPL facility in order to experimentally explore the effect of time dependent prepulses on the target backside emission. The setup is shown in figure 15 a. A pair of selectable beamsplitters is used to extract a predetermined fraction of energy out of the beam and recombine with the primary beam path after passage of the delay arm of the interferometer. A translation stage carrying two reflective optics allows for the variation of the pulse delay. Typical results of our study are shown in figure 15 b. Images were taken through our SXR PHC

operating at a magnification of 15. We do not see evidence of increased output intensity or conversion efficiency independent of pulse delay, however, we do note a rather large shot to shot variation.

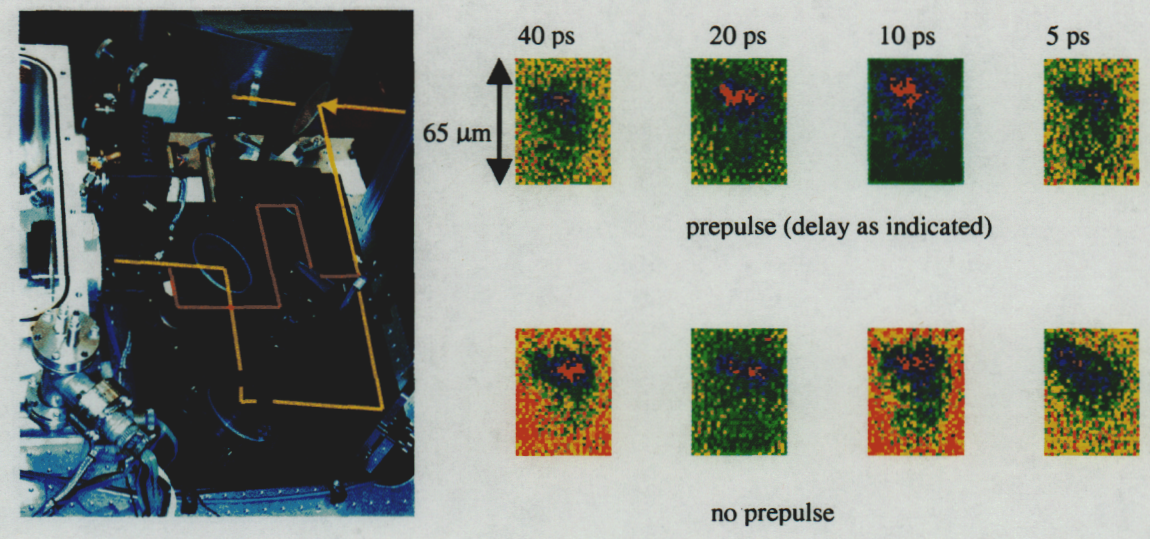

Figure 15 a, b: USPL interferometer suitable for adjusting pump probe delay.
Relative focal spot intensities taken with SXR PHC.

Apart from intentional pulse trains, short-pulse lasers are often superimposed on a longer duration, lower-intensity pedestal of amplified spontaneous emission (ASE). This ASE prepulse can also affect the interaction of the main laser pulse, and in some ultra-high intensity experiments we assume that ASE may even produce a substantial preformed plasma in front of the solid target. However, the conditions where ASE becomes relevant have not been well investigated. Preplasma formation threshold intensities quoted in recent literature, on the order of 10^{11} W/cm^2 [40], arise from the assumption that ASE cannot affect the main interaction unless the field intensity is sufficient to cause plasma breakdown on the solid target. Recent experiments [41] provide some evidence that peak ASE intensity is not the only appropriate parameter, and a more comprehensive analysis of the prepulse duration and the target material is required to understand the effect of the

ASE. In figure 16, we present a schematic of typical pulse shapes prevalent in our experiments.

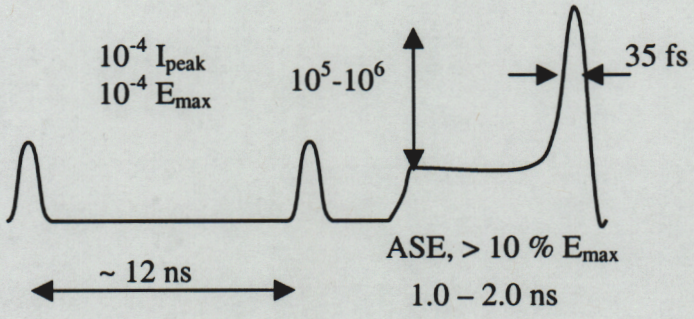

Figure 16: Schematic of typical experimental pulse shape.

Two prepulses, due to leakage of the laser regenerative amplifier, exhibit an intensity of 10^{-4} of the pulse peak intensity and contain 10^{-4} of the maximum pulse energy. They are temporally separated by approximately 12 ns and followed by a low-intensity pedestal of ASE carrying sometimes more than 10 % of the maximum pulse energy. The contrast was determined to be 10^{-5} to 10^{-6} in a best case scenario. We estimate that both, preplasma formation as well as low density vapor blow-off are likely to occur before coupling of the 35 fs main pulse.

6. Summary and Future Directions

We have set out to pursue a longstanding goal of x-ray laser research, the realization of the inner-shell photo-ionization (ISPI) pumping scheme in order to demonstrate lasing at wavelengths not yet possible by table-top energy sources. In this quest we have come to successfully achieve our primary objectives by designing and optimizing an efficient x-ray converter/filter package and studying its backside x-ray emission. For that purpose we have devised and fabricated a versatile soft x-ray spectrometer universally suitable for analysis of various x-ray sources based on laser produced plasmas. A soft x-ray pinhole camera has been used as an additional diagnostic to verify focal spot properties and target intensities. We found a maximum conversion

efficiency of 1.2×10^{-4} at a position of 300 μm out of best focus. We did not see any evidence for increased backside x-ray emission as a result of intentional prepulses delivered to the target, independent of pulse delay.

We have also invented a novel technique to measure the rise time of ultrafast x-ray pulses, which constitutes an enabling technology in the diagnosis of modern 4^{th} generation light sources currently under design worldwide. There, we employ a diamond x-ray transducer in a pump probe arrangement to reflect a p-polarized probe beam at Brewster's angle. In addition, we have shown how to create a line focus using an ultrashort optical laser pulse in traveling wave geometry employing a holographically produced grating for compensation of optical aberrations in the relay imaging system, which are introduced by the use of standard spherical and cylindrical components.

On a slightly dismal note, a significant number of co-investigators and collaborators have departed from LLNL during the course of this project and replacements have been scarce at best. The Falcon USPL facility was subject to operational safety reviews in FY99, which resulted in complete facility shutdown for several months. Consequently, we experienced delays in the setup process and some of the proposed experiments had to be taken off the schedule.

From a financial perspective, an overall amount of 93 % of funds requested have been allocated. In FY01, resulting from the situation described above, a fraction of only 45.3 % of the annual budget has been expended.

For the near future, we plan to execute the described pump probe experiment at the JANUSP facility at LLNL and, based on the success of our investigations in this project, follow an invitation to shoot x-ray laser targets after implementing our traveling wave pumping scheme at another USPL facility. Further down the road, we anticipate that the properties that can be expected from ISPI XRLs, such as brightness, ultrashort pulse duration, coherence and small divergence will render them ideally suited to biological imaging applications, where biological specimens could then be studied in their fully hydrated state, without the requirements of staining and fixation. We are currently participating in a comprehensive proposal to the National Science Foundation (NSF), where we detail the image acquisition of an intact, living cell under conditions that are physiologically equivalent to their natural environment using an ISPI XRL.

Acknowledgments

The authors in their capacities as the principle and co-investigators of this project are indebted to a great many contributors over the course of the three-year period of LDRD funding. Without them, successes of this endeavor would not have been possible to the extent described in this document. We would especially like to acknowledge the effort of Troy W. Barbee, Jr., who fabricated all of the multilayer optical elements for our soft x-ray spectrometer; Jim Cox and Phil Waide from the ICF target diagnostics group at LLNL designed and built most all of the mechanical setup for the various target experiments, and Yuelin Li during his tenure at LLNL helped with the initial layout for a traveling wave pumping system. Todd Ditmire and Greg Hayes were instrumental in the installation and everyday operation of the Falcon ultrashort pulse laser facility in the early stages of the experiment while John Crane and Rick Cross assumed that responsibility after the former had departed from LLNL. Ken Wharton provided critical laser alignment and shared his data on the effects of non-ionizing prepulses in high intensity laser-solid interactions, while Jason Zweiback performed amplifier, pulse stretcher and compressor debugging procedures. Luxel Corporation, led by Forbes Powell, manufactured x-ray laser targets including the coatings. We would also like to thank a very accomplished and renowned x-ray laser researcher, Joe Nilsen of A-Division, for his continued support and belief in the project. Finally, we gratefully acknowledge the helpful and sometimes lively discussions and support of physicist in V-, and X-Divisions as well as MTP, including Jim Dunn, Dick Lee, Rich London, and Dennis Matthews.

References

1 D. L. Matthews et al., *Phys. Rev. Lett.* **54**, 110 (1985)

2 S. Suckewer et al., *Phys. Rev. Lett.* **55**, 1753 (1985)

3 J.J. Rocca et al., *Phys. Rev. Lett.* **77**, 1476 (1996)

4 B.E. Lemoff et al., *Phys. Rev. Lett.* **74**, 1574 (1995)

5 Y. Nagata et al., *Phys. Rev. Lett.* **71**, 3774 (1993)

6 P. V. Nickles et al., *Phys. Rev. Lett.* **78**, 2748 (1997)

7 J. Dunn et al., *Phys. Rev. Lett.*, **80**, 2825 (1998)

8 E. Spiller, *Soft X-Ray Optics*, SPIE, Bellingham, WA (1994)

9 M. A. Duguay and P. M. Retzepis, *Appl. Phys. Lett.* **10**, 350 (1967)

10 H. C. Kapteyn, *Appl. Opt.* **31**, 4931 (1992)

11 S. J. Moon and D. C. Eder, in *X-ray lasers 1996*,
S. Svanberg and C. –G. Wahlstrom, eds.
(Institute of Physics Publisher, Bristol, 1996), pp. 143

12 G. L. Strobel et al., *Appl. Phys.* **B 58**, 45 (1994)

13 Y. Li et al., *Opt. Commun.* **144**, 118 (1997)

14 S. J. Moon and D. C. Eder, *Proc. SPIE* **3156**, 326 (1997)

15 M. D. Perry and G. Mourou, *Science* **264**, 917 (1994)

16 M. M. Murnane et al., *Appl. Phys. Lett.* **62**, 1068 (1993)

17 S. P. Gondon et al., *Opt. Lett.* **19**, 484 (1994)

18 R. Marjoribanks et al., *Bull. Amer. Phys. Soc.* **39**, 1519 (1994)

19 C. Wulker et al., *Appl. Phys. Lett.* **68**, 1338 (1996)

20 G. B. Zimmerman and W. L. Kruer,
Com. Plasma Phys. and Cont. Fusion, **2**, 51 (1975)

21 M. E. Mack et al., *Appl. Phys. Lett.* **15**, 166 (1969)

22 R. Wyatt and E. E. Marinero, *Appl. Phys.* **25**, 297 (1981)

23 H. J. Polland et al., *Appl. Phys.* **B 32**, 53 (1983)

24 M. H. Sher et al., *Opt. Lett.* **12**, 891 (1987)

25 C. P. J. Barty et al., *Phys. Rev. Lett.*, **61**, 2201 (1988)

26 Zs. Bor, S. Szatmari, and A. Muller, *Appl. Phys.* **B 32**, 101 (1983)

27 J. C. Moreno, J. Nilsen, and L. B. Da Silva, *AIP Conf. Proc.* **332**, 21 (1994)

28 Z. L. Horvath et al., *Opt. Eng.* **32**, 2491 (1993)

29 J. R. Crespo Lopez-Urrutia et al.: *Proc. SPIE* **2012**, 258 (1993)

30 Z. S. Bor et al., *Opt. Eng.* **32**, 2501 (1993)

31 S. D. Brorson and H. A. Haus, *J. Opt. Soc. Am. B* **5**, 247 (1988)

32 S. Szatmari, G. Kuhnle, and P. Simon, *Appl. Opt.* **29**, 5372 (1990)

33 D. Kühlke et al., *Appl. Phys. Lett.* **50**, 1785 (1987)

34 M. M. Murnane et al., *Phys. Rev. Lett.* **62,** 155 (1989)

35 V. L. Ginzburg, *The Propagation of Electromagnetic Waves in Plasmas* (Pergamon, New York, 1964) p.260

36 F. Brunel, *Phys. Rev. Lett.* **59**, 52 (1987)

37 H. W. K. Tom and O.R. Wood, *Appl. Phys. Lett.* **54**, 517 (1989)

38 S. Bastiani et al., *Phys. Rev.* **E 56**, 7179 (1997)

39 Th. Schlegel et al., *Phys. Rev.* **E 60**, 2209 (1999)

40 B. F. K. Young et al., *Phys. Rev.* **E 58**, 4929 (1998)

41 K. B. Wharton et al., *Phys. Rev.* **E 64** (2), 25401 (2001)

Appendix

I. Lectures and Conference Presentations

"An Inner-Shell Photo-Ionized X-Ray Laser at 45 Å"
F. Weber, P. Celliers, L. Da Silva, S. Moon, and R. Snavely
International Conference on LASERS '99 (invited)
12/4/1999 – 12/10/1999, Quebec City, QB, CANADA

"On the Path Towards a Carbon Inner-Shell X-Ray Laser"
L. B. Da Silva, P. M. Celliers, F. A. Weber, and S. J. Moon
2000 Optical Society of America/Annual Meeting (invited)
10/22/200 – 10/26/2000, Providence, RI

II. Invitations

"Inner-Shell Photo-Ionized X-Ray Lasing at 45 Å"
F. Weber, P. Celliers, L. Da Silva, S. Moon, and R Snavely
2000 OSA/ILS XVI Meeting, 10/22/200 – 10/26/2000, Providence, RI

"New Trends in X-Ray Lasers"
F. Weber, P. Celliers, L. Da Silva, S. Moon, and R Snavely
LASERS 2000, 12/4/2000 – 12/8/2000, Albuquerque, NM